

Leipzig NTZ 6/2001
 LU-ITP 2001/011
 UNITU {THEP {15/2001

May 18, 2001

A lattice study of 3D compact QED at finite temperature

M. N. Chernodub^{1,a}, E. M. Ilgenfritz^{2,b} and A. Schiller^{3,c}

^a ITEP, B. Cherenushkinskaya 25, Moscow, 117259, Russia

^b Institut für Theoretische Physik, Universität Tübingen, D-72076 Tübingen, Germany

^c Institut für Theoretische Physik and NTZ, Universität Leipzig, D-04109 Leipzig,
 Germany

ABSTRACT

We study the deconfinement phase transition and monopole properties in the finite temperature 3D compact Abelian gauge model on the lattice. We predict the critical coupling as function of the lattice size in a simplified model to describe monopole binding. We demonstrate numerically that the monopoles are sensitive to the transition. In the deconfinement phase the monopoles appear in the form of a dilute gas of magnetic dipoles. In the confinement phase both monopole density and string tension differ from semiclassical estimates if monopole binding is neglected. However, the analysis of the monopole clusters shows that the relation between the string tension and the density of monopoles in charged clusters is in reasonable agreement with those predictions. We study the cluster structure of the vacuum in both phases of the model.

1 Introduction

Compact Abelian gauge theory in three Euclidean dimensions is a case where permanent confinement is proven and qualitatively understood [1, 2]. In order to gain some experience for more realistic theories, it is interesting to study how this mechanism ceases

¹maxim@heron.itep.ru

²ilgenfri@alpha1.tphysphysik.uni-tuebingen.de

³Arwed.Schiller@itp.uni-leipzig.de

to work under special conditions. High temperature is such a case. In this paper we are going to revisit the finite temperature deconfinement phase transition. We will emphasize the aspect of monopole binding which explains the breakdown of confinement. In a companion paper, we extend these studies to the case of non-vanishing external fields.

Compact QED theory possesses Abelian monopoles as topological defects appearing due to the compactness of the gauge group. Considering the 3D theory as the static limit of a 4D theory, the monopoles are just magnetic monopoles at rest, and the components of field strength are magnetic. In a three dimensional theory, the monopoles are instanton-like objects: instead of tracing world lines (as they do in 4D) they occupy points. The plasma of monopoles and anti-monopoles can explain the permanent confinement of oppositely charged electric test charges [1] in bound states, kept together by a linear potential. In the language of magnetostatics, confinement appears due to the screening of the magnetic field induced by the electric current circulating along the Wilson loop. Monopoles and anti-monopoles form a polarized sheet of finite thickness ("string") along the minimal surface spanned by the Wilson loop. The formation of the string (observed in the lattice simulations in Ref. [3]) leads, for non-vanishing electric current, to an excess of the free energy proportional to the area.

At finite temperature the phase structure becomes non-trivial. What we have in mind, is compactifying $3D \rightarrow (2+1)D$ in the "temporal" (third or z) direction. The confinement-deconfinement phase transition was studied on the lattice both analytically [4] and numerically [7]. According to the Svetitsky-Ya e universality arguments [5], an interpretation of the transition has been attempted in terms of the $U(1)$ vortex dynamics of the corresponding 2D spin system. The phase transition which is expected to be of the Kosterlitz-Thouless type [6] was demonstrated to be accompanied by restructuring of the vortex system [7]. The vortices are described by a 2D $U(1)$ spin model representing the dynamics of the Polyakov line (see also the discussion in Ref. [4]). Approaching the transition temperature, vortices and anti-vortices start to form bound states. In the high temperature phase no unbound vortices and anti-vortices are left.

In the present paper we discuss an interpretation of deconfinement starting from the confinement picture outlined above, in terms of magnetic monopoles. The confinement plasma of the monopoles and anti-monopoles turns into the dipole plasma at the deconfinement phase transition. The dipole plasma is inefficient to completely screen the field created by the electric currents running along the pair of Polyakov lines. In this case the screening mass vanishes while the magnetic susceptibility of the "medium" is smaller than unity. Both monopole and vortex binding mechanisms of the deconfinement phase transition have been discussed for 3D finite temperature Georgi-Glashow model in Refs.[8] and [9], respectively.

In the finite temperature case, strictly speaking, there is a problem to call all the fields "magnetic" as we did above when we summarized the zero temperature case. Similar to Ref. [7], the confinement aspect itself will be illuminated in terms of the $U(1)$ valued Polyakov lines in the third direction and of Polyakov line correlators representing pairs of charges separated in 2D space. In $(2+1)D$ there is no symmetry anymore between the three components of the field strength tensor. The closest relative of the true magnetic field is F_{12} distinct from the others, while there is still a symmetry between F_{13} and F_{23} . With this distinction in mind one can conditionally call them the "magnetic" and

"electric" components of the field strength tensor, respectively. As long as one does not introduce external fields, even at finite temperature there is no need to distinguish between them. The sources of the respective fluxes will be simply called "monopoles" or "magnetic charges" in the following.

The binding of the monopoles is not isotropic. It happens mainly in the 2D space direction due to the logarithmic potential between the monopoles separated by a large spatial distance. As a consequence of the periodic boundary conditions in the temporal direction the force between the monopoles and anti-monopoles vanishes at half of the temporal extent. Therefore the potential in the temporal direction is weaker than in the spatial directions. As a consequence, the spatial size of the monopole bound state is expected to be smaller than the size in the temporal direction. This means that the dipoles are dominantly oriented parallel or antiparallel to the 3rd direction. The monopole deconfinement scenario raises the question whether the monopole properties (such as pairing and orientation) could be influenced by an eventual external field. This aspect will be addressed in a companion paper.

With or without external field, the deconfinement mechanism by monopole pairing seems to have interesting counterparts in more realistic gauge theories. The formation of monopole pairs is qualitatively similar to the binding of instantons in instanton molecules with increasing temperature in QCD suggested to be responsible for chiral symmetry restoration [10]. In the electroweak theory, the formation of Nambu monopole-anti-monopole pairs, a remnant from a dense medium of disordered Z-vortices and Nambu monopoles which characterizes the high temperature phase, is accompanying the transition towards the low temperature phase [11]. Note also, that a dipole vacuum, although not confining, still has a non-perturbative nature [12].

The plan of the paper is as follows. In Section 2 we estimate the critical coupling of the confinement-deconfinement phase transition based on a monopole binding model for a finite lattice. In the next Section the transition is numerically located for a lattice size $32^2 \times 8$ and confinement properties are studied. We present various monopole properties including dipole formation based on a cluster analysis in Section 4. We study the relation of the monopoles and dipoles to the phase transition in Section 5. We briefly summarize our results in the last Section.

2 Some heuristic considerations

In 3D compact electrodynamics there are monopoles interacting via the Coulomb potentials,

$$S = \frac{g_m^2}{2} \sum_{a,b} q_a q_b V_T(\mathbf{x}_a, \mathbf{x}_b); \quad (1)$$

where q_a and \mathbf{x}_a are, respectively, the charge (in units of the elementary monopole charge, $g_m = 2/g_3$, where g_3 is the three dimensional coupling constant) and the 3D position vector of the a^{th} monopole. The subscript T indicates that the interaction potential V_T eventually depends on the temperature.

At zero temperature the monopoles are randomly located in the Euclidean R^3 space and the classical interaction potential between the monopole and anti-monopole is inversely proportional to the distance R between the objects, $V_0(R) = (4\pi R)^{-1}$. At finite temperature T the monopoles live in the $R^2 \times S_1$ space (with S_1 being a circle of perimeter T^{-1}) and the interaction potential gets modified. At small separations between monopole and anti-monopole the interaction is zero (temperature like), $V_T(\mathbf{x};z) = V_0(\sqrt{x^2 + z^2}) + \dots$, where $\mathbf{x} = (x;y;z) = (x;z)$. At large spatial separations x the potential between monopoles is essentially two-dimensional [8],

$$V_T(\mathbf{x};z) = -2T \ln |x| + \dots; \quad |x| \gg T^{-1} \quad (2)$$

However, the interaction between monopoles separated by a distance z in the third (temperature) direction is of the 3D Coulomb type for small spatial inter-monopole distances, $|x| \ll T^{-1}$: $V_T(\mathbf{x};z) = (4\pi z)^{-1}$, $z \ll T^{-1}$. The force between monopoles and anti-monopoles at a distance $z = 1/(2T)$ vanishes due to periodicity in the temperature direction. Thus one might expect that at finite temperature the monopoles form magnetically neutral states which are bounded in the spatial directions. However, the dynamics of the monopoles in the temperature direction is not restricted by a logarithmic potential.

Thus, at zero temperature the system exists in the form of a Coulomb gas of magnetic monopoles and anti-monopoles. In this phase the medium contains electric charges [1]. As temperature increases, the three-dimensional Coulombic potential turns into a two-dimensional logarithmic potential for spatial monopole interactions. The monopoles and anti-monopoles become weakly bound and form more and more dipole bound states. The dipoles have a finite average spatial size (the distance between the magnetically oppositely charged constituents) which is a decreasing function of the temperature since the interaction potential between the particles rises as temperature increases, cf. eq. (2).

In the low temperature regime, this dipole size would be still larger than the average distance between the particles inside the plasma, and therefore only a small fraction of monopoles residing in actual dipoles is mixed with an weakly correlated monopole-anti-monopole component. At sufficiently large temperature, however, the typical dipole size becomes smaller than the interparticle distance in the plasma and the system turns into a pure dipole plasma. The conformational property is closely related to the Debye mass generation effect which is absent in the pure dipole plasma [13]. As a consequence, the conformational of electrically charged particles disappears. The system experiences a conformational-deconformation phase transition due to the monopole binding mechanism.

One can use these heuristic arguments to estimate the phase transition temperature. In continuum theory this analysis was done in Ref. [8] where compact electrodynamics was represented as a limit of the Georgi-Glashow model. The phase transition in this theory happens at a temperature $T = g_3^2/(2\pi)$. This result has been obtained under the condition that the average size of the effective magnetic dipole is not an infrared divergent quantity as it is the case in the conformational phase.

However, in lattice gauge theory the considered quantities are all finite and the considerations should be modified compared to the continuum case. The difference between monopole and dipole plasmas can only be seen if the mean distance r between the constituent monopoles becomes comparable to the dipole size d . The distance r can be expressed via the density of the monopoles ρ , as $r = \rho^{-1/3}$. Thus, the phase transition

happens when the dipole size and the average distance between monopoles become of the same order,

$$d = \ell^{1/3}; \quad (3)$$

where ℓ is a geometrical factor of order unity. For both quantities, d and ℓ , estimates can be easily obtained on the lattice while the factor ℓ is to be defined from a simulation.

We consider the 3D compact U(1) gauge model on the $L_s \times L_t$ lattice with the action written in the Villain representation:

$$Z = \sum_{\{n\}} \int \prod_{\langle ij \rangle} d\theta_{ij} \exp \left[-\frac{v}{2} \sum_{\langle ij \rangle} (n_{ij} - \theta_{ij})^2 \right]; \quad (4)$$

where θ_{ij} is the compact U(1) gauge field and n is the integer-valued auxiliary tensor field variable. v is the Villain coupling constant.

To relate this to the numerical simulations, we also consider the formulation of the compact U(1) gauge theory with Wilson action:

$$S = \sum_P \left[1 - \cos \theta_P \right]; \quad (5)$$

The Villain coupling constant v is related to the Wilson coupling β as follows [14]:

$$v(\beta) = -2 \log \frac{I_0(\beta)}{I_1(\beta)}; \quad (6)$$

where $I_{0;1}$ are the standard modified Bessel functions.

The partition function (4) can be rewritten in the following "grand canonical" form, i.e. represented as a sum over monopole charges in the (dual) lattice cubes [14]:

$$Z / Z_{\text{mon}} = \sum_{\{m\}} \exp \left[-2 \sum_{c_3} v(m; \Delta^{-1} m) \right]; \quad (7)$$

Here Δ^{-1} is the inverse of the Laplacian operator on an asymmetric lattice, m_c denotes the monopole charge in the cube c_3 . The inverse Laplacian for lattice sizes L_s, L_t is given as follows:

$$\Delta^{-1}(\mathbf{x}; L_s; L_t) = \frac{1}{2L_s^2 L_t} \sum_{\mathbf{p}^2 \neq 0} \frac{e^{i(\mathbf{p} \cdot \mathbf{x})}}{3 \prod_{i=1}^3 \cos p_i}; \quad (8)$$

where $p_{1;2} = 0; \dots; 2$ ($L_s - 1$)= L_s and $p_3 = 0; \dots; 2$ ($L_t - 1$)= L_t .

In order to estimate the average distance between the monopole and anti-monopole constituents in a dipole state (i.e., the dipole size) we use the "canonical" monopole-anti-monopole (dipole) partition function which can be easily read off from eq. (7):

$$Z_{\text{dip}}^{(2)} = \text{const} \sum_{\mathbf{x}} \exp \left[-4 \sum_{c_3} v \left[\Delta^{-1}(\mathbf{x}; L_s; L_t) - \Delta^{-1}(0; L_s; L_t) \right] \right]; \quad (9)$$

the sum extends over all lattice separations x between m monopole and anti(m monopole). The zero distance between these objects is excluded (since this case does not correspond to a dipole state). The rms. dipole size d is given by

$$d^2(\nu; L_s; L_t) = \frac{1}{Z_{\text{dip}}^{(2)}} \sum_x x^2 \exp \left[-\frac{4\nu}{2} x^2 \right] \langle \rho(x; L_s; L_t) \rho(0; L_s; L_t) \rangle; \quad (10)$$

where the actual distance squared, x^2 , is evaluated taking into account the periodic boundary conditions of the lattice. The sum cannot be taken analytically.

The monopole density can be read off from eq.(7),

$$\langle \rho; L_s; L_t \rangle = 2 \exp \left[-\frac{4\nu}{2} \right] \langle \rho(0; L_s; L_t) \rangle; \quad (11)$$

where the dependence on the lattice geometry is indicated explicitly. Note that in this formula no interaction between monopoles is taken into account and we refer to it as to "bindingless". Only the local "self-interaction" of monopoles is accounted for via the Coulomb propagator $\rho(0)$ in the fugacity. We are discussing the binding effects on the monopole density in Section 5.

The geometrical factor is to be defined from the numerical data. To this end we assume that this factor is a constant quantity which does not depend on the lattice extensions. Indeed, it gives an estimate how large the intradipole distances should be compared to the monopole density in order to have the dipole field screened. This is a quite strong assumption which, however, turns out to be reasonable, as will we see below. To define the factor we substitute eqs. (10) and (11) into eq. (3) and use numerical values for ρ_c presented in Ref. [7]. For the lattices $16^2 \times L_t$, $L_t = 4; 6; 8$ we get, respectively: $\rho_c = 0.723(58); 0.622(47)$ and $0.646(116)$. These numbers coincide with each other within numerical errors. Taking the average over L_t we get $\rho_c = 0.63$. In what follows we take

$$\rho_c = 0.63; \quad (12)$$

and then solve eqs.(3,11,10) with respect to the Villain coupling ν . Then we finally estimate the critical Wilson coupling β_c^{th} with the help of eq. (6). The results for lattices of various sizes are represented in Table 1 and compared with pseudocritical couplings

	$L_s = 16$		$L_s = 32$		$L_s = 64$
L_t	β_c^{th}	ρ_c	β_c^{th}	ρ_c	β_c^{th}
4	1.87	1.83(2)	2.01	-	2.10
6	2.04	2.08(2)	2.26	2.18(3)	2.44
8	2.12	2.14(5)	2.39	2.30(2)	2.62

Table 1: The critical coupling constant β_c^{th} calculated using eqs. (6,3,10,11,12) for different lattices $L_s^2 \times L_t$ compared to lattice Monte Carlo results of Ref. [7]. Note that our results for the lattice $32^2 \times 8$ are slightly higher than that of Ref. [7], see forthcoming Sections.

ρ_c obtained in lattice simulations of Ref. [7]. The agreement between the data and our estimates is within 4%. Thus the simple heuristic arguments based on the monopole-dipole picture work surprisingly well.

3 Phase transition and confinement

We have performed our numerical study of (2+1)D compact electrodynamics using the Wilson action (5). The lattice coupling is related to the lattice spacing a and the continuum coupling constant g_3 of the 3D theory as follows:

$$= \frac{1}{ag_3^2}; \quad (13)$$

Note that in three dimensional gauge theory the coupling constant g_3 has dimension $mass^{1/2}$.

The lattice corresponding to the finite temperature is asymmetric, $L_s^2 = L_t$, $L_t < L_s$. In the limit $L_s \rightarrow \infty$ the "temporal" extension of the lattice L_t is related to the physical temperature, $L_t = 1/(Ta)$. Using eq. (13) the temperature is given via the lattice parameters as follows:

$$\frac{T}{g_3^2} = \frac{1}{L_t}; \quad (14)$$

Thus, at fixed lattice size lower (higher) values of the lattice coupling constant correspond to lower (higher) temperatures.

Our simulations have been performed mainly on a $32^2 \times 8$ lattice. We do not intend to study in the present paper finite size scaling aspects of this model. The local Monte Carlo algorithm is based on a 5-hit Metropolis update sweep followed by a microcanonical sweep. For better ergodicity, in particular in the presence of an external field (considered in a companion paper), also global updates are included. Following the ideas of Ref. [15], the global refreshment step consists in an attempt to add an additional unit of flux with randomly chosen sign in a direction randomly selected among the three, to the dynamical gauge field subject to a global Metropolis acceptance check.

For example, one unit of flux in ij plane is introduced with the help of the following gauge field shift [15] $\tilde{A}_i = [A_i + \tilde{A}_i]_{mod 2}$:

$$\begin{aligned} \tilde{A}_j &= \frac{1}{L_i} (2x_i - L_i - 1); \quad \tilde{A}_j = 0 \text{ for } x_j \notin L_j; \\ \tilde{A}_i &= \frac{2}{L_i L_j} (1 - x_j); \quad \tilde{A}_k = 0; \quad k \notin \{i, j\}; \end{aligned}$$

The acceptance rate of the global step changes within the considered range from roughly 0.7 (confinement phase) to 0.2 (deconfinement phase). One total Monte Carlo update cycle consists of two combined local Metropolis and microcanonical sweeps (requiring an acceptance rate of 0.5 for the Metropolis step) and the global update described above.

In order to localize the deconfinement transition, it is convenient to study the expectation values of the two bulk operators,

$$\langle L_j \rangle = \frac{1}{L_s^2} \int_{x=0}^{L_s} L(x) dx; \quad \langle L_i \rangle = \frac{1}{L_s^2} \int_{x=0}^{L_s} L(x) dx; \quad (15)$$

constructed from the Polyakov loop,

$$L(x) = \exp \left[i \sum_{z=1}^n \int_{x=0}^{L_s} \mathcal{L}_3(x; z) dz \right]; \quad (16)$$

here $\mathbf{x} = (x; y)$ is a two-dimensional vector. In the deconfined phase the quantity $|\mathbf{L}|$ is of the order of unity, while in the confined phase it is close to zero in a finite volume and vanishes in the infinite volume limit.

The behaviour of the expectation value of the Polyakov loop vs. lattice coupling is shown in Figure 1 (a). The low temperature phase, $\beta < \beta_c$ corresponds to the confined

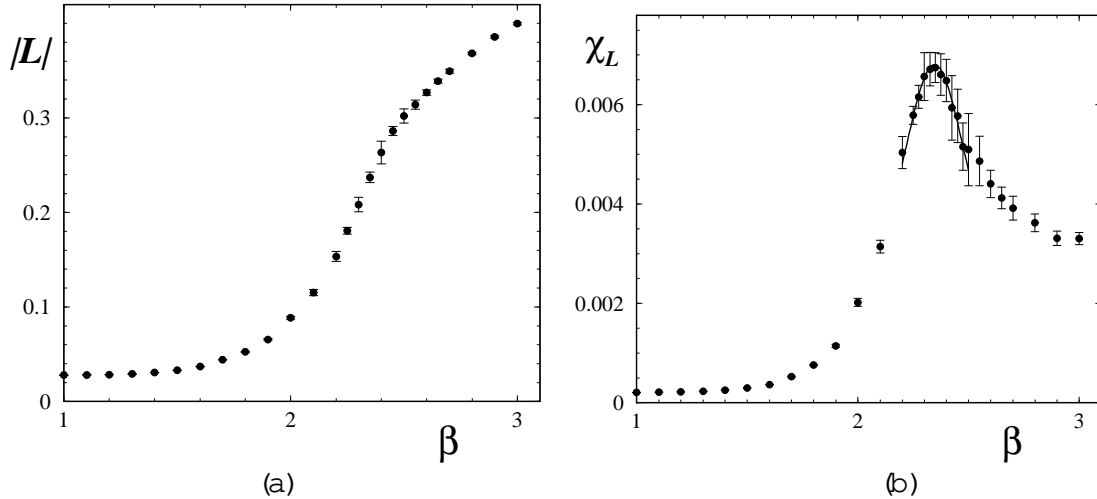


Figure 1: (a) The expectation value of the absolute value of the average Polyakov loop (15) and (b) its susceptibility (17) vs. β .

phase, while the high temperature phase is deconfined.

The susceptibility of the Polyakov loop

$$\chi_L = \langle |\mathbf{L}|^2 \rangle - \langle |\mathbf{L}| \rangle^2 \quad (17)$$

is shown in Figure 1 (b). The peak of the Polyakov loop susceptibility corresponds to the pseudocritical β_c of the deconfined phase transition. We have fitted the susceptibility near its maximum by the following function:

$$\chi_L^t(\beta) = \frac{c_1^2}{c_2^2 + (\beta - \beta_c)^2}; \quad (18)$$

where the critical coupling was estimated to be $\beta_c = 2.346(2)$ which is quite close to the result of Ref. [7]. The best fit is shown in Figure 1 (b) by a solid line.

To calculate the string tension we use $\langle \text{plane} \{ \text{plane} \rangle$ correlators of two Polyakov loops. In addition, averages of temporal Wilson loops have been studied, too. More precisely, in $(2+1)D$, we define first sums of the Polyakov loops along a line parallel to a spatial lattice axis (e.g. in the y direction):

$$L_{\text{plane}}(\mathbf{x}) = \prod_{y=1}^{\mathbf{x}_s} L(\mathbf{x}; y); \quad (19)$$

The correlator of the plane-plane correlators may be written as a sum of point-point correlation functions,

$$\langle L_{\text{plane}}(0) L_{\text{plane}}(\mathbf{x}) \rangle = \sum_{y_1, y_2=1}^{\mathbf{x}_s} \langle L(0; y_1) L^+(\mathbf{x}; y_2) \rangle; \quad (20)$$

The form of this correlator is expected to be:

$$\langle L_{\text{plane}}(0)L_{\text{plane}}(x) \rangle = \text{const} \frac{1}{\cosh L_t x} \left(\frac{L_s}{2} \right)^x; \quad (21)$$

where L_t is the "temporal" string tension. In Figure 2 (a) we show the fit of the Polyakov

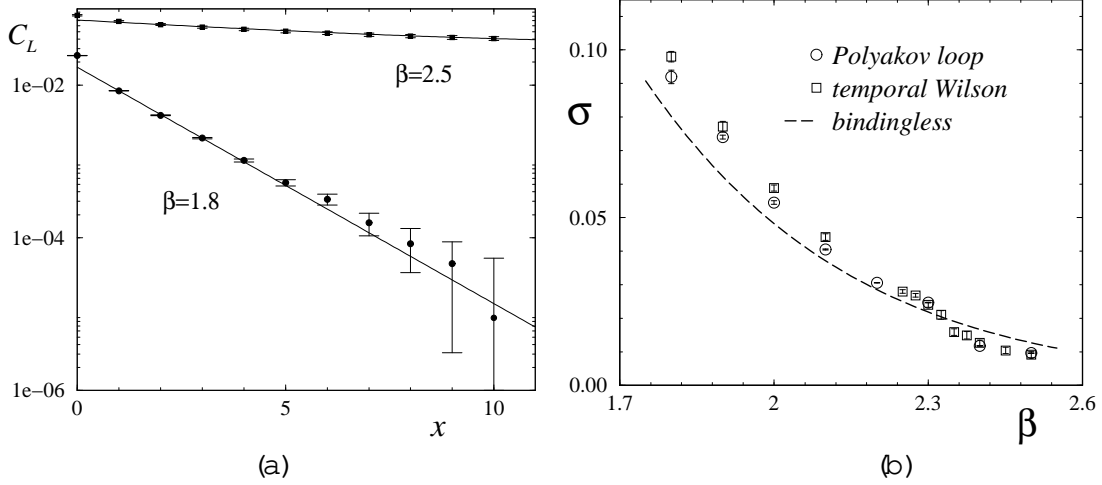


Figure 2: (a) Fit of the Polyakov plane correlator (20) using eq. (21) in the confinement, $\beta = 1.8$, and deconfinement, $\beta = 2.5$, phases. (b) String tensions as functions of β compared with the bindingless theoretical result (22).

plane correlator (20) by this fitting function in the confinement ($\beta = 1.8$) and deconfinement ($\beta = 2.5$) phases, respectively.

In Figure 2 (b) we present the fitted string tensions as function of β . Above β_c the string tension quickly drops down but stays non-zero due to finite volume effects. The temporal string tensions obtained using either the Polyakov loop plane correlators or the temporal Wilson loop averages roughly coincide with each other. The dashed curve represents the theoretical prediction for the string tension [14, 16]:

$$\sigma(\beta) = \frac{4^{\frac{p-2}{2}}}{v(\beta)} \exp \left[-\frac{2}{v(\beta)} \left(\frac{L_s}{2} \right)^x \right]; \quad (22)$$

A good agreement between the prediction and the numerical results is reached only in the vicinity of the phase transition point, $\beta \approx 2.3$. In order to understand these differences, we turn now to a closer investigation of the monopole properties.

4 Properties of the monopole-anti-monopole system

The basic quantity describing the behaviour of the monopoles is the monopole density, $\rho_c = \langle \sum_c n_c \rangle / (L_s^2 L_t)$, where n_c is the integer valued monopole charge inside the cube defined in the standard way [17]:

$$n_c = \frac{1}{2} \sum_{P \in \partial c} (-1)^P [P]_{\text{mod } 2}; \quad (23)$$

where the plaquette orientations relative to the boundary of the cube are taken into account. The density of the total number of m monopoles is a decreasing function of the lattice coupling β (or the temperature) as it is shown in Figure 3 by circles. At high

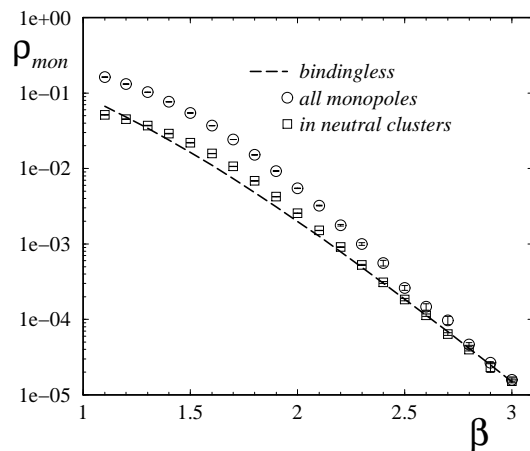


Figure 3: The density of all m monopoles and of m monopoles in neutral clusters vs. β .

temperatures (large β) the m monopoles are dilute and form dipole bound states. Typical m monopole configurations in both phases are visualized in Figure 4.

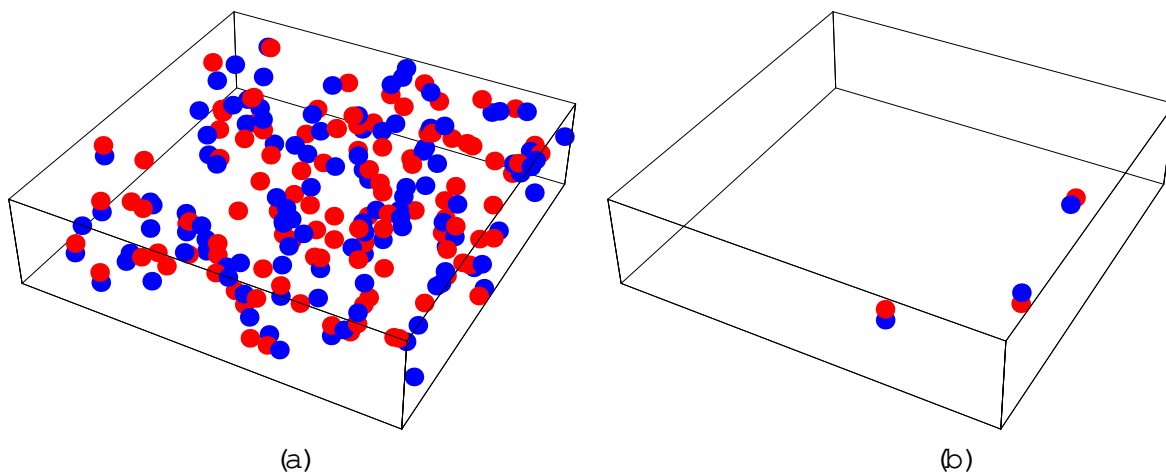


Figure 4: Typical m monopole configurations for (a) the confinement phase ($\beta = 1.6$) and (b) the deconfinement phase ($\beta = 2.5$).

In Figure 3 we show by the dashed line the density of the m monopoles calculated using eq. (11) for comparison. As in the case of the string tension, the predicted m monopole density is in agreement with the numerical data only near β_c .

Equation (11) is based on the single m monopole contribution to the partition function, thus it does not take into account pairing of the m monopoles. The effect of the constituent

m onopole pairing (dipole formation) due to finite temperature can explain the deviations from the bindingless case seen in this Figure. In the con nem ent phase the density of the m onopoles is larger than the prediction of eq. (11). Indeed, we expect that the formation of the bound state decreases the total energy (action) of the chosen m onopole and anti{m onopole. As a result binding favours the creation of additional m onopoles by quantum uctuations. This tendency increases with larger β , however the cost of creating new m onopoles grows, too.

Note that the entropy of the bound state is smaller than the entropy of a free m onopole and an anti{m onopole. However the entropy e ect does not seem to change essentially near the phase transition.

We remind the reader that on the classical level the dipoles are formed both in the con nem ent phase and in the decon nem ent phase due to logarithmic potential between the m onopoles. However, at low temperatures the dipole size is larger than the average distance between the m onopoles and, therefore, the dipole formation does not destroy con nem ent.

One can analyse the m onopole pairing studying the cluster structure of the m onopole ensemble extracted from the Monte Carlo con gurations. For our purposes, clusters are defined as follows: clusters are connected groups of m onopoles and anti{m onopoles, where each object is separated from at least one neighbour belonging to the same cluster by a distance less or equal than R_{max} . In the following we use $R_{max}^2 = 3a^2$ which means that neighbouring m onopole cubes should share at least one single corner^a. Note that the increase of the coupling constant leads not only to an increase of the temperature, eq. (14), but to a decrease of the lattice spacing a as well, eq. (13). Thus at different the same characteristic distance R_{max} corresponds to different physical scales. Therefore our results below are of only qualitative nature.

A m onopole cluster is neutral if the charges of the constituent m onopoles sum up to zero. We show the density of m onopoles belonging to neutral clusters as a function of β in Figure 3 by squares. The difference between this density and the total m onopole density amounts to a factor three at $\beta = 1$ and becomes smaller at larger β . At large β (entering the decon nem ent phase) approximately every second m onopole or anti{m onopole belongs to a neutral cluster. At still larger β 's almost all m onopoles are in neutral clusters.

We are confident that the uctuation of m onopole numbers signal the decon ning phase transition. This is demonstrated studying the second and (modified) fourth Binder cumulants of the total number of m onopoles and anti{m onopoles [and of the number of (anti){m onopoles being part of neutral clusters]. We present in Figure 5 the cumulants, with M_i denoting the respective number :

$$B_2 = \frac{M^2_i}{M_i^2} - 1 \quad (24)$$

$$B_4 = \frac{M^4_i}{3M^2_i} - \frac{1}{3}; \quad (25)$$

Similarly to the Polyakov line susceptibility these quantities are suitable to localize the

^a In Ref.[18] a similar definition has been used to investigate tightly packed clusters with $R_{max} = a$. In our case the condition for the cluster is more relaxed.

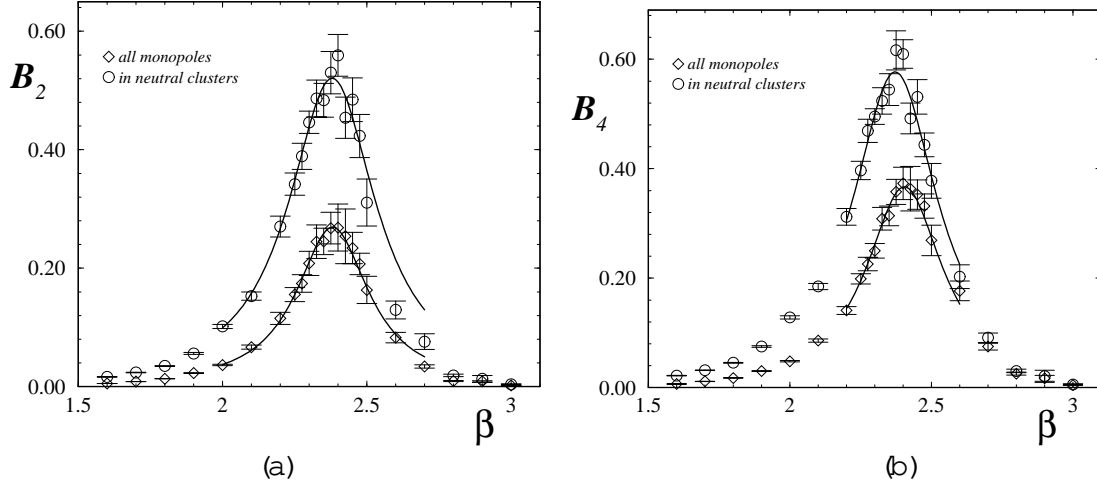


Figure 5: The second (a) and the fourth Binder (b) cumulants according to (25) for the total (anti)monopole density and the corresponding densities enclosed in neutral clusters. The fits are shown as solid lines.

deconfining phase transition. We fit these cumulants by

$$B_n^t(\beta) = \frac{c_1^2}{c_2^2 + (\beta - \beta_c)^2}; \quad n = 2; 4: \quad (26)$$

The fits are shown by solid lines in Figure 5 and the results for the pseudocritical couplings β_c are given in Table 2.

cumulant	2nd	4th
total	2.380 (3)	2.404 (4)
neutral	2.379 (5)	2.372 (3)

Table 2: Pseudocritical couplings β_c from the fits to the Binder cumulants (25,26).

Some details on the cluster structure at various values of β can be seen in Figure 6 (a). We show the fraction of monopoles and anti-monopoles being part of clusters of size N . The cluster size is the number of monopoles and anti-monopoles which belong to the given cluster. There is no separation according to the cluster's charge. In the confinement phase, $\beta = 1.5$, the fraction of monopoles is slowly decreasing with the cluster size N . The percentage of isolated (anti)monopoles ($N = 1$ clusters) amounts to roughly 45% while clusters (with a size up to $N = 10$) contain the rest.

At the phase transition point ($\beta = 2.3$) the number of (anti)monopoles enclosed in larger clusters drops drastically. The monopole vacuum is composed mostly of individual (anti)monopoles (60%) and dipoles (40%). This observation can be reconciled with our theoretical expectation that all monopoles must become paired only if we accept that the "unpaired" monopoles are actually part of dipoles of size bigger than R_{max} . Deeper in the deconfined phase, however, at $\beta = 2.8$ practically 90% of the (anti)monopoles form tight bound states with sizes smaller than $R_{max} = \sqrt{3} a$.

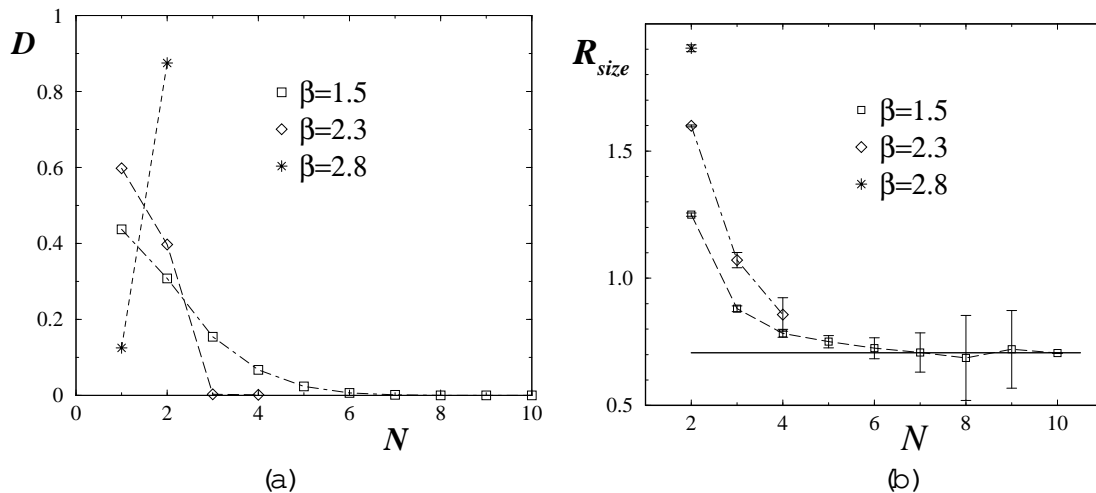


Figure 6: (a) The cluster structure at various of the coupling constant β . Cluster distribution is shown as a function of the number of constituent monopoles inside clusters, N . (b) The cluster shape function, eq. (27), for various β .

As we have discussed above, we expect that the force in the spatial directions is larger than the force along the temporal direction z . This fact can be qualitatively analysed with the help of the following "cluster sphericity":

$$R_{size}(N) = \frac{\langle r_z^2 \rangle_N}{\langle r_x^2 \rangle_N + \langle r_y^2 \rangle_N}; \quad (27)$$

where $\langle r_x^2 \rangle_N$ is the average distance from the center of the cluster in x direction etc. for cluster size N . If the clusters are elongated predominantly in the temporal direction this quantity would be larger than unity, and smaller otherwise. We show the dependence of the sphericity R_{size} on the cluster size N for various β values in Figure 6 (b). Small clusters are directed predominantly along the temporal direction, as expected, at all β . With larger β the elongation becomes stronger. For large clusters the direction of the cluster is random, since in this case the cluster shape function is very close to $1/\sqrt{2}$ (this directly follows from the definition (27)). This random limit is marked by the solid line in Figure 6.

5 Concomitant and monopoles

We have observed that agreement between predictions from a theory without monopole binding and the finite temperature simulation results is reached only in the vicinity of the phase transition point, $\beta = 2.3$. In the concomitant phase both measured temporal string tension and monopole density are larger compared to the bindingless predictions, see Figures 2 (b), 3.

As we have discussed, it is due to monopole binding that the density of the monopoles is increased compared to the non-interacting case. However, the size of the dipoles in the concomitant phase is larger than the average distance between the ordinary monopoles

calculated from their total density. Therefore, the monopoles bound in dipoles due to classical logarithmic potential still give a contribution to the string tension.

It is interesting to check how the monopole density fits into the theoretical predictions of the string tension (22). Using that predicted relation, we compare in Figure 7 the ratio

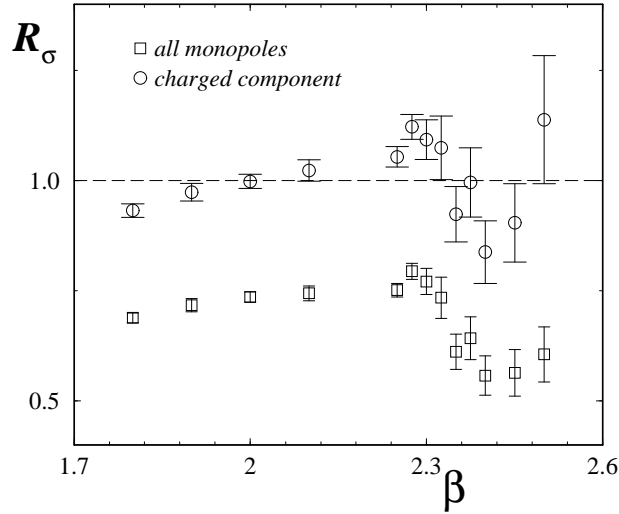


Figure 7: The ratio of the temporal string tensions (28) vs. β .

R between the measured string tension (from plane-plane correlators of Polyakov loops) with a calculated "theoretical" string tension t_h using as input the measured monopole density :

$$R = \frac{t}{t_h} : \tag{28}$$

Here t_h is given in accordance to eqs.(11,22) via

$$t_h = \frac{4}{v} \frac{\langle \sum_{\mu} \langle \text{tr} U_{\mu} \rangle \rangle}{\langle \text{tr} U \rangle} ; \tag{29}$$

and v is defined in eq. (6).

The circles shown take into account all "active" monopoles, i.e. isolated ones and those from charged monopole clusters which might be thought to be responsible for the string tension. The ratio is close to unity indicating the fact that the charged monopoles provide the major contribution to the string tension, as expected. Note that in the deconfinement phase the string tension is non-zero due to finite size effects discussed below. The squares in Figure 7 (a) are related to the ratio (28) in which all monopoles are taken into account. In both phases this ratio is smaller than unity: a neutral fraction of the monopoles bound in the small dipole pairs does not contribute to the string tension.

The small "string tension" remaining after passing the deconfinement transition at this finite lattice can be explained from the point of view of the dipole picture as follows. Test particles separated by distances smaller than sizes of certain dipoles are influenced by the constituent monopoles of those dipoles. The monopoles give contribution to the

string tension term. On the finite lattice the maximal distance between the test particles is of the order of the lattice size. Therefore, dipoles of the same size could be responsible for the non-vanishing small string tension. Dipoles of these sizes may really be present in the deconfinement phase (with a probability decreasing with the increase of the lattice size). This, however, does not contradict the criterion used to locate the phase transition in the previous Sections since the dipoles of such large size are heavily suppressed.

The dipole formation due to Coulomb forces also happens at zero temperature. This effect increases the monopole density compared to that in the "bindingless" world. To check this we compare in Figure 8 the total density of the total density of monopoles and

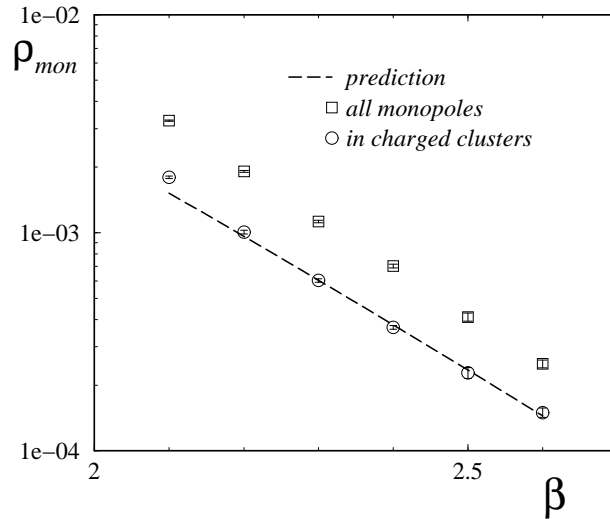


Figure 8: The density of all monopoles and of monopoles in charged clusters vs. β for a 32^3 lattice compared to prediction (11).

the exclusive density of monopoles residing in charged clusters (the latter includes free monopoles and anti-monopoles) for a 32^3 lattice. The charged monopoles comprise around 55% of the total monopole density. This ratio does not depend on the value of the coupling constant indicating that the scaling behaviour of charged and neutral clusters is the same. The charged fraction of the monopoles is perfectly described by the "bindingless" formula (11) for the monopole density. This formula is incorporated implicitly into the theoretical prediction of the string tension (22) which works well according to Ref. [19]. Thus only the monopoles from the charged clusters (including separate monopoles) contribute to the string tension while the binding effect causes the appearance of a large fraction of "inactive" neutral clusters.

Finally, we have measured the "spatial string tension": the coefficient in front of the area term in the spatial Wilson loops. This string tension σ_s has been obtained by means of the standard diagonal Creutz ratios. The results are presented in Figure 9 as a function of β . As expected, the spatial string tension does not vanish and behaves smoothly across the deconfining phase transition. In contrast, we show in this Figure also the "true" temporal string tension extracted from temporal Wilson loops which drops down to the level of the finite-volume correction that we have just discussed.

At sufficiently high temperatures the system might be treated as two-dimensional with

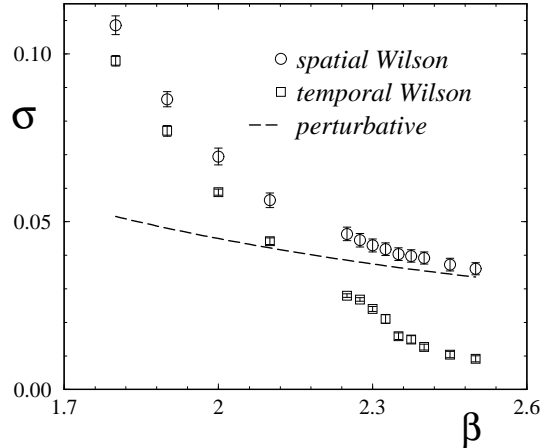


Figure 9: The spatial string tension vs. β .

an effective 2D coupling constant $L_t^{(2D)}$. Moreover, since the monopole density is low at large β (in deconfinement), the model becomes effectively noncompact. Thus the spatial Wilson loop behaviour in this regime is given by the perturbative one (photon exchange). In two dimensions the Coulomb law provides the linearly confining potential, $V^{(2D)}(R) \propto R$, corresponding to the spatial string tension,

$$\sigma_s^{th}(\beta) = \frac{1}{2 L_t^{(2D)}} = \frac{1}{2L_t} ; \quad (30)$$

which is shown in Figure 9 by the dashed line. The spatial string tension data and the curve approach each other for sufficiently large β . However, in the confinement phase the monopoles give a significant contribution to the spatial string tension.

6 Summary

In this paper we have considered a mechanism of the finite temperature deconfinement phase transition in three dimensional compact electrodynamics based on the monopole binding. The considerations are similar to those given in Ref. [8] for the continuum theory and they incorporate features of the lattice geometry. This allows us to predict the pseudocritical coupling as a function of the lattice size.

In our numerical simulations we have demonstrated that the monopoles are sensitive to the phase transition despite the fact that the monopole density itself behaves smoothly across the transition. The pseudocritical couplings found by the Binder cumulants of the density are very close to that identified using the Polyakov loop susceptibility. We stress that we did not intend to study the finite size scaling behavior of this model.

Based on the observation to find β_c in this way we have studied the monopole properties in more detail. We have found that both the monopole density and the string tension differ from the predictions based on a model which does not take into account the monopole binding effects. However we have found numerically that the ratio between these two

quantities derived in that model (given by eq. (22)) remains valid in the confinement phase.

We have observed that the dipole formation happens both in the confinement and deconfinement phases. In the deconfinement phase tightly bound dipoles which are safely identified by a cluster algorithm dominate in the vacuum. The dipoles are oriented dominantly in the temporal direction. These features are in agreement with general expectations discussed in the Introduction and in Section 2.

At the confinement phase transition we observe mostly clusters with two constituents or single monopoles and anti-monopoles. Decreasing further the temperature (or β), the monopoles become dense and form connected clusters (on a coarser and coarser lattice) enclosing various numbers of monopoles and anti-monopoles. The largest clusters are more and more spherical. Whether the observed properties of the dipole gas formation survives in the continuum limit deserves an additional study.

When the phase transition is mediated by charged objects, one could expect that external fields will influence the phase transition. In our case the natural question arises what will happen to the confinement/deconfinement phase transition. For non-Abelian theories in $3+1$ dimensions it was recently concluded, from a study of the expectation value of the Polyakov loop [20], that confinement seems to become restored under the influence of an external chromomagnetic field. In an accompanying paper [21] we will report on a study of our model under such external conditions, concerning the influence of confinement and relevant properties of the monopole system.

Acknowledgements

Authors are grateful to P. van Baal, M. I. Polikarpov and J. Zaanen for interesting discussions. M. N. Ch. acknowledges a support of Sächsisches Staatsministerium für Kunst und Wissenschaft, grant 4-7531.50-04-0361-01/16 and kind hospitality of NTZ and the Institute of Theoretical Physics of Leipzig University. Work of M. N. Ch., was partially supported by grants RFBR 99-01230a, RFBR 01-02-17456 and CRDF award RP1-2103. E. M. J. acknowledges the support by the Graduiertenkolleg "Quantenfeldtheorie" for a working visit to Leipzig.

References

- [1] A. M. Polyakov, Nucl. Phys. B 120 (1977) 429.
- [2] M. G. Opfer and G. Mack, Commun. Math. Phys. 82 (1981) 545.
- [3] T. Sterling and J. Greensite, Nucl. Phys. B 220 (1983) 327.
- [4] N. Parga, Phys. Lett. B 107 (1981) 442.
- [5] B. Svetitsky, Phys. Rept. 132 (1986) 1.
- [6] J. M. Kosterlitz and D. J. Thouless, J. Phys. C 6 (1973) 1181.

- [7] P.D.Coddington, A.J.Hey, A.A.Middleton and J.S.Townsend, *Phys. Lett. B* 175 (1986) 64.
- [8] N.O.Agasian and K.Zarembo, *Phys. Rev. D* 57 (1998) 2475.
- [9] G.Dunne, I.I.Kogan, A.Kovner and B.Tekin, *JHEP* 0101 (2001) 032
- [10] T.Schafer, E.V.Shuryak, J.J.M.Verbaarschot, *Phys. Rev. D* 51 (1995) 1267;
R.Rapp, T.Schafer, E.V.Shuryak and M.Velkovsky, *Annals Phys.* 280 (2000) 35;
E.M.Ilgenfritz and E.V.Shuryak, *Phys. Lett. B* 325 (1994) 263
- [11] M.N.Chemodub, F.V.Gubarev and E.M.Ilgenfritz, *Phys. Lett. B* 424 (1998) 106;
M.N.Chemodub, F.V.Gubarev, E.M.Ilgenfritz and A.Schiller, *Phys. Lett. B* 443 (1998) 244; *ibid.* B 434 (1998) 83.
- [12] M.N.Chemodub, *Phys. Rev. D* 63 (2001) 025003; hep-th/0011124; B.L.Bakker,
M.N.Chemodub and A.I.Veselov, *Phys. Lett. B* 502 (2001) 338; I.I.Kogan,
A.Kovner and B.Tekin, *JHEP* 0103 (2001) 021.
- [13] J.Glimm and A.Jaeger, *Comm. Math. Phys.* 56 (1977) 195.
- [14] T.Banks, R.Meyerson and J.Kogut, *Nucl. Phys. B* 129 (1977) 493.
- [15] P.H.Daamgaard and U.M.Heller, *Nucl. Phys. B* 309 (1988) 625.
- [16] J.Ambjorn, A.J.Hey and S.Otto, *Nucl. Phys. B* 210 (1982) 347.
- [17] T.A.DeGrand and D.Toussaint, *Phys. Rev. D* 22 (1980) 2478.
- [18] Z.Schram and M.Teper, *Phys. Rev. D* 48 (1993) 2881.
- [19] R.J.Wensley and J.D.Stack, *Phys. Rev. Lett.* 63 (1989) 1764.
- [20] P.Cea and L.Cosmai, hep-lat/0101017.
- [21] M.N.Chemodub, E.M.Ilgenfritz and A.Schiller, in preparation